



Effect of nano-scale, reduced graphene oxide on the degradation of bisphenol A in real tertiary treated wastewater with the persulfate/UV-C process



Goksin Ozyildiz, Tugba Olmez-Hanci, Idil Arslan-Alaton*

Istanbul Technical University, School of Civil Engineering, Department of Environmental Engineering, 34469, Maslak, Istanbul, Turkey

ARTICLE INFO

Keywords:

Bisphenol A
Persulfate UV-C activation
Reduced graphene oxide
Degradation products and toxicity
Real tertiary wastewater

ABSTRACT

In this study, the effect of home-made, reduced graphene oxide (rGO) nanoparticles on persulfate (PS)/UV-C oxidation of bisphenol A (BPA; 8.8 μ M), an endocrine disruptor and model micropollutant, in real tertiary treated urban wastewater (TWW) was examined. Experimental results revealed that the presence of rGO induced a significant improvement in the degradation of BPA by the PS/UV-C treatment system. Fast and complete BPA removal accompanied with 44% dissolved organic carbon (DOC) abatement was achieved within 30 min at reaction conditions of 0.01 g/L rGO, 0.125 mM PS, at the natural pH of the TWW (pH = 7.5). This high performance on BPA degradation at the natural pH TWW could be attributable to the synergistic effect between the rGO nanoparticles and the PS/UV-C photochemical oxidation causing additional activation of PS and adsorption of BPA, DOC and degradation products onto the rGO surface. Radical quenching studies revealed that sulfate radicals prevailed over hydroxyl radicals. The *Vibrio fischeri* bioluminescence inhibition assay indicated that no toxic degradation products were formed during rGO/PS/UV-C treatment. By liquid chromatography time of flight mass spectrometry (LC-TOF-MS) analysis the formation of thirteen degradation products during PS/UV-C and rGO/PS/UV-C treatment of BPA was confirmed. This study underlined that the combined rGO/PS/UV-C treatment process could offer a sustainable, ecotoxicologically safe and kinetically attractive solution for the effective elimination of micropollutants from waters and wastewaters.

1. Introduction

Bisphenol A (BPA), chemically designated as 2,2-bis(4-hydroxyphenyl) propane, is commonly used as an intermediate in variety products like polycarbonate plastics and epoxy resins [1,2]. Its production had a global market share of 15 billion pounds in 2013 with an annual increase of almost 5% foreseen from 2014 to 2020 [3]. After release during production and consumption, BPA can be transformed or degraded via abiotic and biological processes in the aquatic environment [4].

The concentration of BPA in natural water sources is in the μ g/L–ng/L range, which is by several orders of magnitude under the chronic toxicity threshold. However, estrogenic effects of BPA products on humans and laboratory animals have been proven in previous studies [2,3]. It was also postulated that a long-term human exposure to BPA at low concentrations may lead to liver damage, thyroid hormone disorders, pancreatic-cell function disruption and obesity, increasing the prevalence of cardiovascular disease, diabetes and liver-enzyme

abnormalities [3,5]. Hence, the presence of BPA in the aquatic and terrestrial environment has been considered as a major concern and risk for public health. Conventional water and wastewater treatment is not effective in BPA removal, while advanced treatment methods such as ozonation, activated carbon adsorption or membrane processes have significant removal efficiencies but at extremely high operating and capital costs [6,7]. On the other hand, biological treatment (activated sludge, biofilms) for BPA is not feasible due to slow and inefficient removal rates [1]. Consequently, alternative advanced treatment processes such as “advanced oxidation processes” (AOPs) have applied for the oxidative removal of BPA and its degradation products over the last 10–15 years and obtained results were encouraging [2,5,8–12].

Recently, AOPs based on the formation of sulfate radicals ($\text{SO}_4^{\cdot-}$) from persulfate (PS) and peroxymonosulfate (PMS) salts has received growing attention as a promising alternative for the degradation and mineralization of toxic and/or refractory pollutants found in water and wastewater owing to its several advantages such as high reactivity, inherent stability, wide operation range and relatively low costs

* Corresponding author.

E-mail address: arslanid@itu.edu.tr (I. Arslan-Alaton).

[13–16]. PS can be activated via several means such as UV-C, heat, microwave, ultrasound and transition metal ions, metal oxides and zero valent metals. Among these treatment initiators it has been reported that the homogenous PS/UV-C oxidation process is kinetically and technically superior to other, sulfate radical-based AOPs [2,17].

More recently, the use of nanocarbon-based materials in adsorptive and catalytic applications for the removal or destruction of emerging contaminants has also been widely studied [18–22]. Particular graphene has been the focus of recent research due to its high specific surface area, tunable surface behavior, and extremely high electron mobility [23–27]. Graphene-based materials (carbocatalysts) have been used as alternative adsorbents or heterogeneous (photo)catalysts for effective removal or degradation of a range of heavy metals, metalloids and a variety of organic contaminants [28–30]. Parallel to these applications, our previous work has demonstrated that the activation of PS with a non-metallic carbocatalyst, namely reduced graphene oxide (rGO) resulted in the formation of free radicals dominated by $\text{SO}_4^{\cdot-}$, which were capable of complete BPA removal not only in pure water but also in real, tertiary treated wastewater (TWW). It could be demonstrated that the carbonyl (C=O) groups of graphene might activate [31]. PS, however, the treatment mechanism and reaction pathways have not been fully established and understood yet.

It should also be pointed out that attention has been increasingly turned toward the intermediates of BPA degradation through biological, chemical and photochemical treatment processes. BPA's metabolites, chemical degradation intermediates and co-pollutants have been investigated as potential endocrine disruptors, genotoxins and toxicants [2,10]. Some recent work has underlined that some of these degradation products possess toxicity and other adverse bio-effects calling for scientific attention.

As a matter of fact, when new treatment processes are proposed, a more holistic understanding of the risks associated with the use of BPA has become a priority task. Therefore, it is crucial to investigate the nature and toxicity of BPA degradation products before the applicability of emerging treatment process involving a combination of PS, rGO and UV-C radiation can further be questioned. It should also be considered that real water and wastewater matrices are very complex since they bear different inorganic and organic components [8,32]. In real effluent, it might be difficult to anticipate and control the oxidation of micropollutants and its degradation products with the above mentioned, novel treatment systems.

Considering the above mentioned issues, the main objectives of the present experimental study were to (i) evaluate the synergistic effect of home-made rGO nanoparticles on PS/UV-C photochemical treatment of BPA in real TWW; (ii) identify BPA degradation products evolving during the application of PS/UV-C and rGO/PS/UV-C treatment systems to compare and enlighten the degradation pathway; (iii) determine the surface properties of rGO before and after rGO/PS/UV-C treatment of BPA to explain the synergy between rGO, PS and UV-C; (iv) elucidate the dominant reaction mechanism by free radical quenching studies using probe chemicals and (v) measure changes in acute toxicity of BPA during PS/UV-C and rGO/PS/UV-C treatments to compare the ecotoxicological safety of the proposed treatment applications.

To the best of our knowledge, the activation of PS with UV-C in the presence of rGO in real TWW has not yet been reported and thus the treatment mechanism of the combined rGO/PS/UV-C treatment system is still unclear. In addition to the expected PS activation and subsequent $\text{SO}_4^{\cdot-}$ formation by UV-C and eventually rGO, BPA could be more conveniently adsorbed on the rGO surface leading to an enhanced BPA removal efficiency.

Table 1
Environmental characterization of the TWW.

Parameter	Value
BPA (µg/L)	< 3.0
DOC (mg/L)	6.7
COD (mg O ₂ /L)	< 30
BOD ₅ (mg O ₂ /L)	< 1
TSS (mg/L)	< 10
Alkalinity (mg CaCO ₃ /L)	192
Hardness (mg CaCO ₃ /L)	242
UV ₂₅₄ (cm ⁻¹)	0.1216 cm ⁻¹
Color	40 Pt-Co units
Conductivity	846 µS/cm
SO ₄ ²⁻ (mg/L)	97
Cl ⁻ (mg/L)	107
pH	7.6

2. Experimental

2.1. Materials

BPA (228 g/mol; C₁₅H₁₆O₂; CAS Nr: 80-05-7; 99.9%), graphite (C, CAS Nr: 7782-42-5, flakes, 100 mesh) and potassium persulfate (K₂S₂O₈; CAS Nr: 7727-21-1; 99.5%) were purchased from Sigma-Aldrich. Chromatographic grade acetonitrile (CH₃CN; CAS Nr: 75-05-8) was obtained from Merck (Germany). All other chemicals and reagents used in this study were of analytical grade, provided from Merck or Sigma-Aldrich and used as received without further purification.

The TWW effluent sample was taken from a local advanced domestic wastewater treatment plant located in Istanbul, Turkey. It was designed as A2/O process for the removal of organic matter (COD), nitrogen (N) and phosphorus (P). The design capacity of the plant was 200,000 m³/d of domestic wastewater. The characteristics of the TWW sample is presented in Table 1 in terms of collective environmental parameters.

2.2. PS/UV-C and rGO/PS/UV-C treatments and control experiments

UV-C photolysis and UV-C based advanced oxidation (PS/UV-C or rGO/PS/UV-C) experiments were conducted in a LZC-ORG model (Luzchem Research Inc., Canada) reaction chamber (dimensions: 32 × 33 × 21 cm). The photoreactor set-up has been described elsewhere in detail [32]. The average radiation flux of UV-C lamps was measured as 2.6 W/m². The experimental procedure of PS/UV-C and rGO/PS experimental runs are given elsewhere [31,32]. At predetermined time intervals, 2 mL samples were withdrawn and immediately filtered through 0.22 µm membranes to 2 mL HPLC vials pre-filled with 0.5 mL methanol. Membrane filters were used for the separation of rGO particles from the reaction solution, whereas methanol was added to cease the free radical reactions. Experimental conditions used in the present work (rGO and PS concentrations and treatment time) were selected considering previous optimization studies that have been reported elsewhere in detail [31]. It should be pointed out that the selected PS concentration (0.125 mM; 24 mg/L) is well below the effluent discharge limits set for sulfate concentrations in water and wastewater as well [33]. Initial and final pH values of the reaction solutions were measured in all treatability experiments and the pH changes were recorded as less than 0.5. All experiments were carried out in duplicate and whenever unusual or erroneous results were obtained, the experiment was repeated.

2.3. Preparation and characterization of rGO nanoparticles

Flakes of the home-made rGO were thermally reduced and expanded from GO. GO was synthesized according to a modified Hummers' method [23,25,34]. The details for GO and rGO synthesis

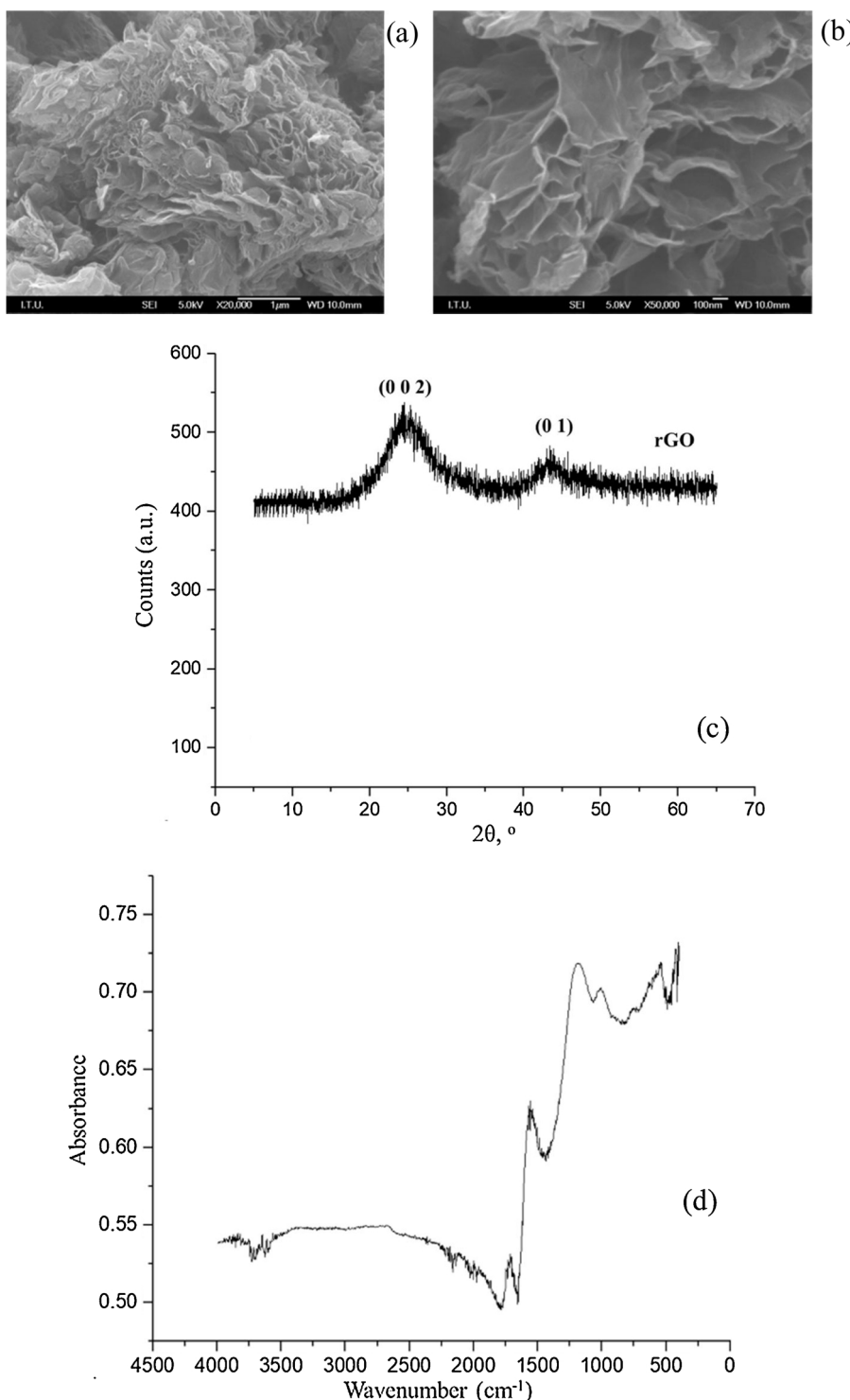


Fig. 1. SEM-EDS images at $\times 20,000$ (a) and $\times 50,000$ (b) magnification, XRD pattern (c) and FTIR spectra (d) of rGO used in the present study.

procedures are available elsewhere [31]. The surface morphology and elemental composition of the synthesized rGO flakes were characterized on a JEOL JSM 7000 F FEG-SEM by scanning electron microscopy (SEM) and energy dispersive spectroscopy (EDS). SEM-EDS images of the synthesized rGO are presented in Fig. 1 (a) and (b). The shape of the rGO flakes indicated an expansion and porous structure formation, with an average composition distribution of 87% C and 13% O₂. The crystal structure of rGO was examined by X-ray diffraction (XRD) with a Philips-1700 X-ray diffractometer, using Cu-K α radiation ($\lambda = 1.5418 \text{ \AA}$). The XRD spectra measured for 2θ ranges of 10° – 90° for rGO is displayed

in Fig. 1(c). (0 0 2) diffraction peaks of $2\theta = 24.87^\circ$ showed the distance between layers, while $2\theta = 43.45^\circ$ described a short range order in the two-dimensional crystal plane (1 0). The calculated values by using Scherrer and Bragg's equations revealed that rGO crystallites had 5–6 layers with 0.36 nm distance, an average of 2 nm height with 7.6 nm diameter layered structures. Brunauer-Emmett-Teller (BET) surface area analysis was conducted on a Quantachrome Nova 2200e by nitrogen sorption at 77 K. The BET surface area of home-made rGO was obtained as $287.52 \text{ m}^2/\text{g}$. The FTIR spectra of the rGO used in the present study was investigated to identify functional groups on a Bruker

Tensor 27 FTIR spectrometer apparatus. Four bands at 1011, 1185, 1563 and 1720 cm^{-1} were observed and related to C–O stretching (alcoxyl groups), C–O/C–OH stretching (epoxyl groups), C=C bond vibrations and C=O carbonyl stretching (Fig. 1(d)).

2.4. Assessment of degradation products

A liquid chromatography-quadrupole time-of-flight-mass spectrometry (LC-QTOF) system in positive and negative mode was used to identify the transformation products of BPA. The LC-MS/MS system consisted of an Agilent Series 1260 HPLC system coupled to an Agilent 6530 Q-TOF MS (Agilent Technologies). Samples collected at different treatment times during the photochemical experiments were directly analyzed without previous pre-concentration. A reversed-phase Poroshell EC C18 analytical column of 3.0 mm \times 150 mm, 2.7 μm particle size was used for separation (Agilent Technologies). A gradient program was used for the mobile phase, combining solvents A (H_2O) and B (methanol:acetonitrile = 50:50, v:v) as follows: 50% B for 0–1 min, 50% B to 95% B from 1 to 2 min, 95% B for 2–3 min and 95% B to 50% B from 3 to 6 min. The flow rate and the injection volume were 0.3 mL/min and 40 μL , respectively, whereas the column oven temperature was maintained at 40 $^{\circ}\text{C}$. The Q-TOF instrument was operated in the 4 GHz High Resolution Mode. Ions were generated using an electro-spray ion (ESI) source with Agilent Jet Stream Technology. The instrumental parameters were; superheated nitrogen sheath gas temperature of 400 $^{\circ}\text{C}$ at flow rate of 13 L/min; capillary, 4000 V; nebulizer, 40 psi; gas temperature, 250 $^{\circ}\text{C}$; skimmer voltage, 65 V; octopole RF Peak, 750 V; and fragmentor (in source CID fragmentation), 200 V. The mass axis was calibrated using the mixture provided by the manufacturer throughout the m/z 50–1000 range. A second sprayer with a reference solution was used for continuous calibration in positive ion mode using the reference masses of 121.0509 and 922.0098 m/z . MS/MS spectra scan rate was 2.00 spectra/sec. The collision energy was optimized to obtain the highest number of fragments. The full mass spectra data recorded were processed with Agilent Mass Hunter Workstation Software (version B.03.01). The structures of degradation products were confirmed based on the molecular ion masses, the spectrograms of the molecular fragments and previous related work.

2.5. Radical quenching studies

Experiments to identify the predominant free radical species in the rGO/PS/UV-C treatment system were conducted by using tert-butyl alcohol (TBA) and ethanol (EtOH) separately as quenching agents of $\text{SO}_4^{\cdot-}$ and HO^{\cdot} . It was reported in previous work that EtOH can capture both HO^{\cdot} and $\text{SO}_4^{\cdot-}$, while TBA is typically being used as a selective HO^{\cdot} scavenger. The alcohols were added at a concentration of 70.4 mM to achieve a TBA:BPA or EtOH:BPA molar ratio of 8000:1 in the reaction solution, which is an average ratio derived from the scientific literature [16,19]. The free radical probe chemical technique relies on the reactivity differences between the formed radical species (HO^{\cdot} , $\text{SO}_4^{\cdot-}$) and the particular alcohol (TBA, EtOH). It has been suggested that EtOH (an α -alcohol) reacts at high and comparable rates with both HO^{\cdot} and $\text{SO}_4^{\cdot-}$, namely with rate coefficients in the ranges of $1.2\text{--}2.8 \times 10^9 \text{ M}^{-1}\text{s}^{-1}$ and $1.6\text{--}7.7 \times 10^7 \text{ M}^{-1}\text{s}^{-1}$ (around 50 times slower) with $\text{SO}_4^{\cdot-}$, respectively. For TBA, on the other hand, the reaction rate coefficient with HO^{\cdot} ($3.8\text{--}7.6 \times 10^8 \text{ M}^{-1}\text{s}^{-1}$) is about 1000 times higher than that with $\text{SO}_4^{\cdot-}$ ($4.0\text{--}9.1 \times 10^5 \text{ M}^{-1}\text{s}^{-1}$). Consequently, the presence of the probe chemical TBA will be more useful in deciding whether HO^{\cdot} or $\text{SO}_4^{\cdot-}$ is dominant, whereas the effect of EtOH will rather serve as supplemental information. Experimental conditions for the quenching studies were identical to the optimized photochemical treatability experiments (BPA = 2 mg/L (8.8 μM); PS = 0.125 mM; rGO = 0.01 g/L; I_0 = 2.6 W/m²; pH = 7.5) with the only difference being the addition of the alcohol (EtOH, TBA = 70.4 mM) to BPA-spiked TWW prior to PS addition.

2.6. Analytical and instrumental methods

BPA was quantified by an Agilent 1100 Series high-performance liquid chromatograph (HPLC) equipped with a diode-array detector (DAD). The chromatographic conditions used for BPA analysis has been described in former work [31]. The instrument detection limit for BPA (100 μL injection volume) was calculated as 3.0 ng/mL. The dissolved organic carbon (DOC) content of the samples was measured on a V_{PCN} analyzer (Shimadzu, Japan). The toxicity towards the photobacterium *V. fischeri* was measured with a BioToxTM test kit (Aboatox Oy, Finland) based on the percent relative luminescence inhibition after an incubation period of 15-minute in accordance with the ISO 11348-3 [35] protocol. The application of *V. fischeri* acute toxicity tests has been described in more detail elsewhere [36]. TWW sample was characterized in terms of conventional environmental parameters according to APHA/AWWA/WPCF [37]. Analytical measurements were done in triplicate and the standard deviations for the measurements were found to be within the ranges given by the methods' specific procedures.

3. Results and discussions

3.1. Effect of rGO on PS/UV-C treatment

Fig. 2(a) depicts BPA abatement in TWW during PS/UV-C and rGO/PS/UV-C treatments under optimized reaction conditions and the natural pH of the TWW sample. From the figure it is apparent that BPA was

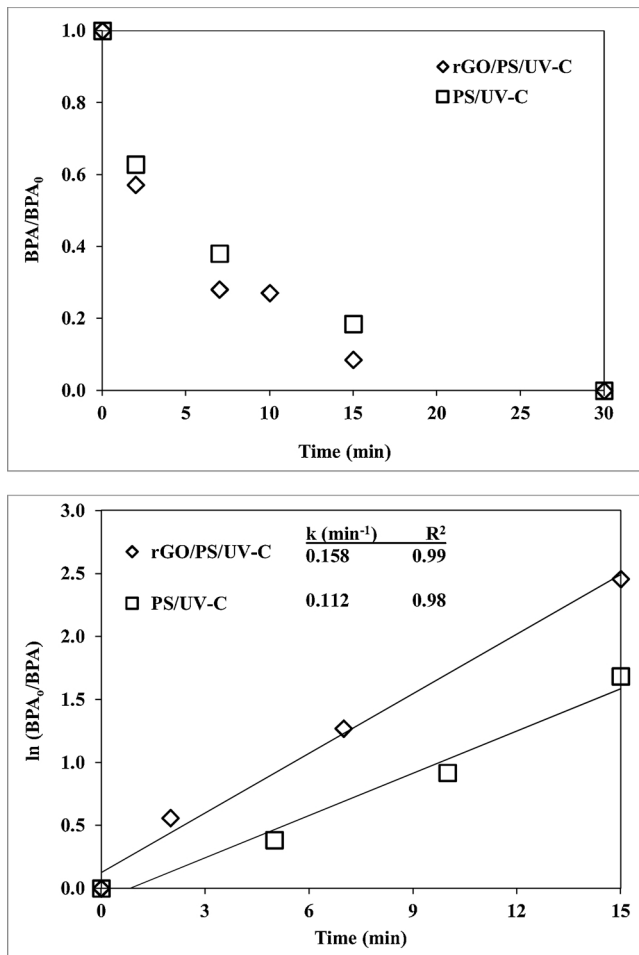


Fig. 2. Normalized BPA (a) and BPA logarithmic (b) plots during PS/UV-C and rGO/PS/UV-C treatments of BPA-spiked TWW. Reaction conditions: BPA = 2 mg/L (8.8 μM); DOC (BPA + TWW) = 8.6 mg/L; PS = 0.125 mM; rGO = 0.01 g/L; I_0 = 2.6 W/m²; pH = 7.5.

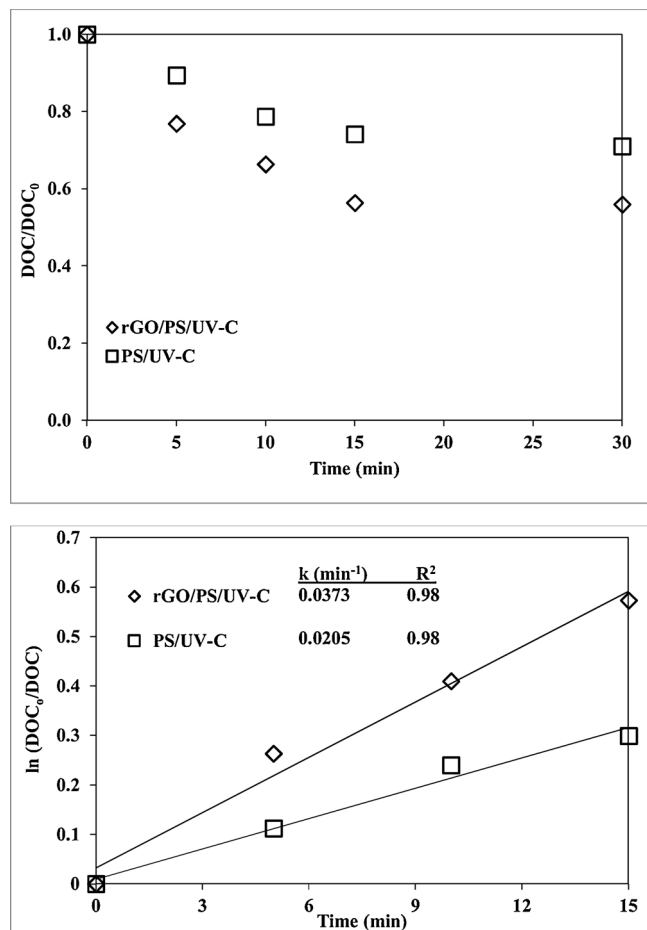


Fig. 3. Normalized DOC (a) and DOC logarithmic (b) plots during PS/UV-C and rGO/PS/UV-C treatments of BPA-spiked TWW. Reaction conditions: BPA = 2 mg/L (8.8 μ M); DOC (BPA + TWW) = 8.6 mg/L; PS = 0.125 mM; rGO = 0.01 g/L; I_0 = 2.6 W/m²; pH = 7.5.

very fast and complete in 30 min for both treatment processes, and an appreciable enhancement in the BPA removal rate was evident upon rGO addition. The enhancement was better reflected upon the pseudo-first order kinetic rate coefficients that perfectly fitted BPA abatements. Fig. 2(b) presents the semi-logarithmic plots for BPA degradation with PS/UV-C and rGO/PS/UV-C treatments together with the respective rate coefficients being inserted into the figure. From the values of the BPA abatements rate coefficients it is evident that the BPA removal rate was enhanced by 41% upon rGO addition. The synergy between rGO and the PS/UV-C photochemical treatment system is also clear from Fig. 3(a) showing changes in DOC (the dissolved organic carbon content of BPA + TWW) for the same photochemical treatment processes. DOC removal was enhanced appreciably upon rGO addition for the PS/UV-C treatment system, however; it slowed down and practically stopped after 15 min treatment, most probably due to the accumulation of oxidation intermediates [32,38]. According to Fig. 3(b), the DOC removal rate was enhanced by 82% in the presence of rGO on the basis of DOC abatement rate coefficients that are also incorporated in Fig. 3(b). After 30 min treatment, 29% and 44% overall DOC removals were achieved with the PS/UV-C and rGO/PS/UV-C treatment processes, respectively. It should be considered that various wastewater ingredients found in the TWW sample such as humic materials (humic, fulvic acids), carboxylic acids, photochemical and biochemical degradation products may contribute to the total DOC and affect DOC and BPA removals with the rGO/PS/UV-C and PS/UV-C treatment processes. Further, inorganic components found in the wastewater such as chloride, bicarbonate, sulfate and phosphate may also inhibit and/or

promote DOC and BPA removals [32], rendering the interpretation of obtained findings rather difficult. In previous works, different results were obtained for the effects of wastewater components on mother pollutant and organic carbon (DOC) abatements; in some cases oxidation inhibition was observed, whereas in other studies no effect or even a positive, accelerating effect was reported [32,38,39] due to the possible interaction between the wastewater ingredients, mother pollutant, its photochemical/photocatalytic degradation products and the active oxidants of the studied treatment processes (SO_4^{2-} ; HO^{\cdot} , etc.). This interaction and the possible positive or negative effects of wastewater components on BPA and DOC removals are expected to be rather complex.

Hence, further mechanistic studies and control experiments would be required to understand the effect of rGO and its interaction with PS/UV-C treatment. The removal mechanisms are mainly thought to be a consequence of oxidation via SO_4^{2-} formed by PS/UV-C and adsorption onto rGO as well as could be concluded from the forthcoming control experiments.

3.2. Control experiments

Several control experiments (UV-C, PS, rGO, rGO/UV-C and rGO/PS treatments) were carried out to explain the synergy between rGO and PS/UV-C and results are displayed in Fig. 4 for BPA (a) and DOC (b) abatement rates. Upon comparison of the control experiments UV-C

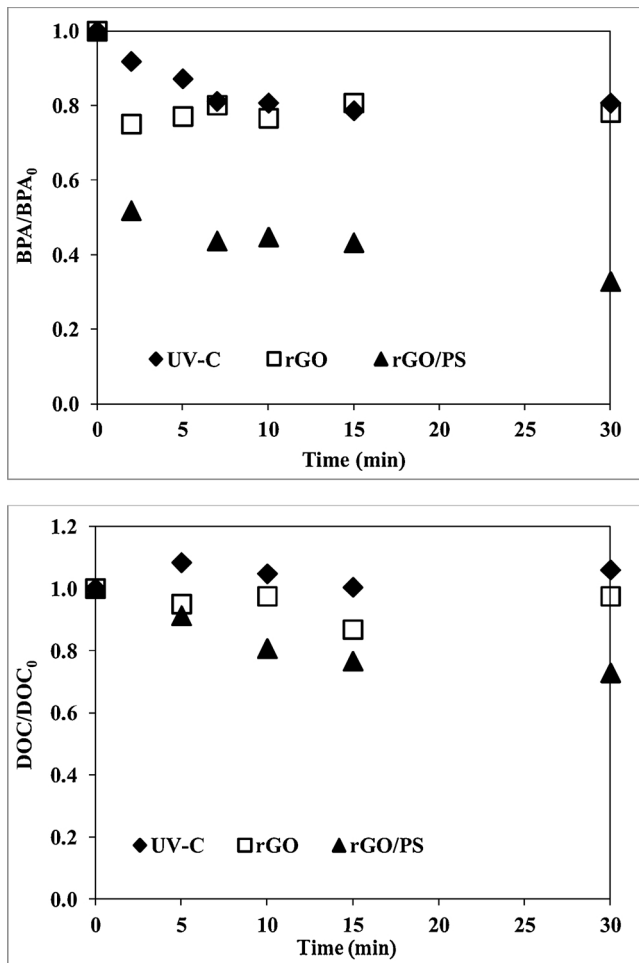


Fig. 4. Normalized BPA (a) and DOC (b) plots during UV-C, rGO and rGO/PS control experiments with BPA-spiked TWW. Reaction conditions: BPA = 2 mg/L (8.8 μ M); DOC (BPA + TWW) = 8.6 mg/L; PS = 0.125 mM; rGO = 0.01 g/L; I_0 = 2.6 W/m²; pH = 7.5.

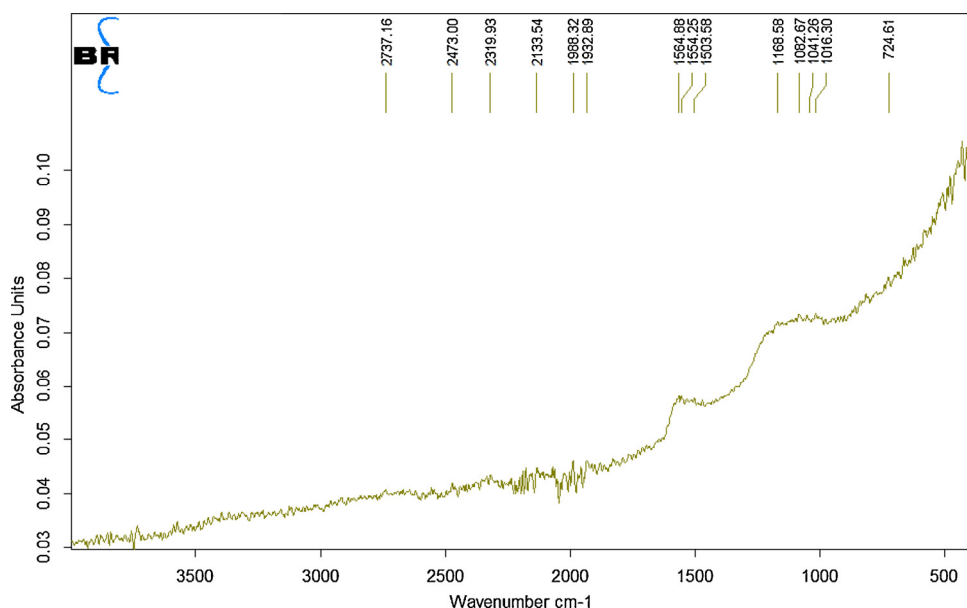


Fig. 5. FTIR spectra of rGO after rGO/PS/UV-C treatment of BPA-spiked TWW.

photolysis, rGO adsorption and rGO/PS oxidative treatment under otherwise identical reaction conditions with the baseline experiments. As can be seen from Fig. 4(a) only slow and poor BPA removals could be achieved by UV-C photolysis; as expected, only 19% BPA removal occurred via UV-C treatment. When the BPA-spiked TWW was subjected to rGO only, a similar overall removal efficiency limited to 22% was obtained; however, this reduction in BPA was attributable to the adsorption of BPA onto the rGO surface at $t = 0$ (“preliminary adsorption”), since BPA already dropped to 1.47 mg/L at $t = 0$ min in the filtrate of the rGO-treated sample. After that and throughout rGO treatment, no further/additional BPA removal was evident (Fig. 4). On the other hand, BPA removal continued during rGO/PS treatment and the BPA removal efficiency increased from 44% due to preliminary rGO adsorption (evidenced after direct filtration of rGO from the $t = 0$ sample) to 67% in total at the end of rGO/PS treatment, speaking for an additional, relative BPA removal of 0.48 mg/L (41% relative BPA removal) during rGO/PS treatment. From the above results it is apparent that BPA abatement by rGO treatment could be surface adsorption, whereas in the presence of PS, PS activation by rGO to form SO_4^{2-} occurs initiating an oxidation reaction mechanism. A relatively slow but distinct BPA abatement was evident throughout rGO/PS treatment of BPA in TWW supporting its removal by a destructive/oxidative process. Although BPA removal was slow and incomplete with rGO/PS, from the results of rGO and rGO/PS treatment it can be concluded that rGO acts an adsorbent and activator during BPA treatment in the absence and presence of PS, respectively. BPA removal via UV-C photolysis accounted for 22%, and 42% BPA removal occurred with rGO/UV-C treatment, that is practically equal to BPA removal with rGO (22%) + UV-C (19%) only, speaking for a merely additive effect of the rGO/UV-C process on BPA removal (i.e. BPA removal by UV-C photolysis + rGO adsorption). BPA reduction by PS treatment was < 10% speaking for insignificant BPA oxidation with un-activated PS in TWW. Although PS has a high oxidation potential (2.1 eV vs SHE) it is not sufficient to degrade wastewater ingredients and BPA under mild operating conditions [17].

1.6 mg/L DOC of the TWW originated from the addition of 2 mg/L BPA, and the DOC content of the TWW was approximately 7 mg/L (6.7 mg/L), making up a total DOC of 8.6 mg/L for BPA + TWW. From the DOC values given in Fig. 4(b) it can be seen that no significant DOC removal (< 20%) occurred due to adsorption onto the rGO surface. Considering preliminary BPA abatements, the initial DOC removal

could mainly be attributed to the reduction in BPA being spiked into TWW. No DOC removal was observed during UV-C treatment and negligible mineralization for rGO (2%) treatment of the BPA-spiked TWW. Again, parallel to the BPA treatment results for the above mentioned control experiments it can be inferred that BPA and organic constituents were mineralized to some extent during rGO/PS treatment; 27% DOC removal was achieved for the rGO/PS control experiment. The higher DOC removal achieved with rGO/PS was probably due to the activation of PS with rGO to produce reactive oxygen species, as has already been reported recently [31].

3.3. Assessment of the rGO surface after rGO/PS/UV-C treatment

In related previous studies the reusability of carbocatalysts was discussed by conducting several consecutive cycle treatability experiments [20–22,31]. Although the efficiency of carbocatalyst-activated PS treatment systems was found to be comparable to conventional metal-based catalyst activation, the stability was reduced even after the first cycle, requiring a significant improvement [20–22,31]. The deactivation of the carbocatalyst was attributed to the intricate influences of surface chemistry and structural changes, including adsorption of intermediates, coverage of surface active sites, changes in pore structures and deterioration of the catalyst properties in the highly oxidative, harsh environment [22,27,29,30]. In the present study, in order to evaluate changes in chemical composition, rGO samples were characterized by FTIR before (Fig. 1(d)) and after (Fig. 5) rGO/PS/UV-C treatment. Results showed that the chemical composition of rGO catalyst was modified during photochemical oxidation. The FTIR bands at 1011, 1185, 1563 and 1720 cm^{-1} were still evidenced after rGO/PS/UV-C treatment; however, their intensities were reduced, speaking for surface oxidation of rGO.

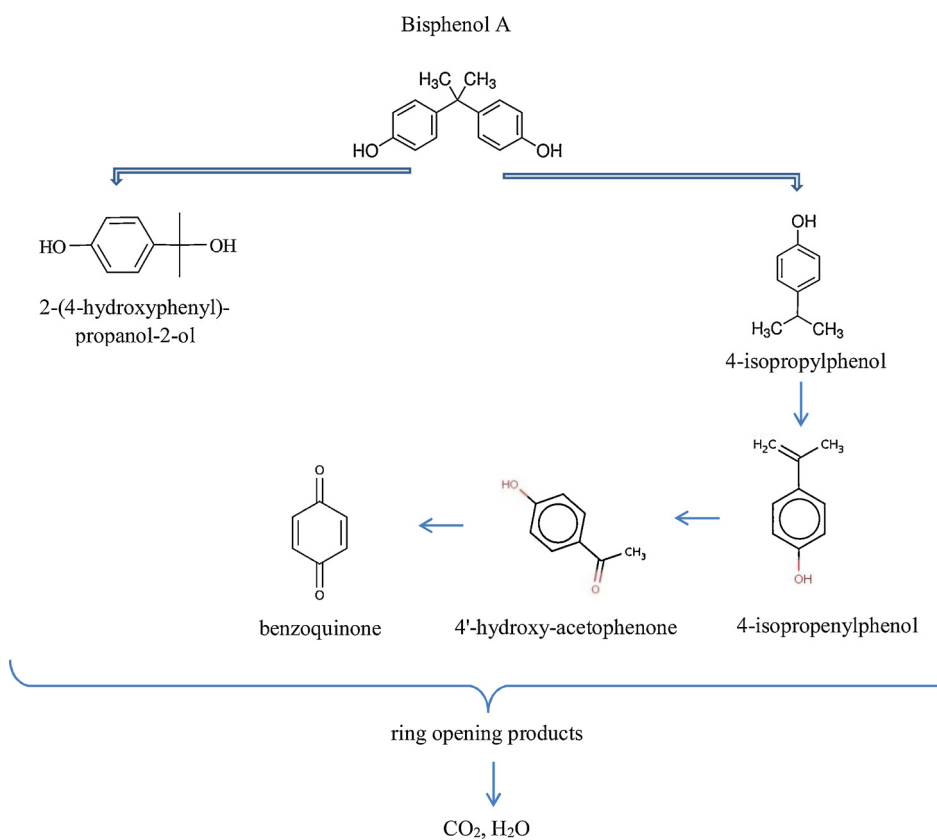
3.4. Assessment of degradation products

In PS activated oxidation processes, depending on the reaction conditions, HO^{\cdot} and SO_4^{2-} are the main active species and might lead to different BPA degradation pathways. As indicated in the related literature, HO^{\cdot} and SO_4^{2-} can oxidize organic pollutants through electron transfer, hydrogen abstraction and substitution mechanisms [17,38]. However, there might have differences in degradation pathways of organic pollutants with these radicals. For example, HO^{\cdot} are more

Table 2

Degradation products obtained during PS/UV-C and rGO/PS/UV-C treatment of BPA in TWW.

Degradation Products	Molecular weight (g/mol)	Molecular formula	Tentative structure	Treatment Process									
				PS/UV-C					rGO/PS/UV-C				
				0 min	5 min	10 min	15 min	30 min	0 min	5 min	10 min	15 min	30 min
DP1	289	Unknown	Unknown	–	–	–	–	–	✓	✓	✓	✓	✓
DP2	273	Unknown	Unknown	–	✓	✓	✓	✓	✓	✓	✓	✓	✓
DP3	266	Unknown	Unknown	–	–	–	–	–	✓	✓	✓	✓	✓
DP4	234	Unknown	Unknown	✓	–	✓	✓	✓	✓	✓	✓	✓	✓
DP5	232	Unknown	Unknown	✓	✓	✓	✓	✓	–	–	–	–	–
DP6	230	Unknown	Unknown	✓	–	✓	✓	✓	–	–	–	–	–
DP7	212	Unknown	Unknown	✓	✓	✓	✓	✓	–	–	–	–	–
DP8	200	Unknown	Unknown	✓	✓	✓	✓	✓	–	–	–	–	–
2-(4-hydroxyphenyl)-propanol-2-ol	152	C ₉ H ₁₂ O ₂		✓	–	–	✓	✓	✓	✓	–	✓	✓
4-hydroxyacetophenone	136	C ₈ H ₈ O ₂		–	–	–	–	✓	–	–	–	–	–
4-isopropylphenol	136	C ₉ H ₁₂ O		–	–	–	–	✓	–	–	✓	✓	–
p-isopropenyl phenol	134	C ₉ H ₁₀ O		–	✓	✓	✓	✓	–	✓	✓	✓	✓
benzoquinone	108	C ₆ H ₄ O ₂		–	–	✓	–	–	–	–	–	–	–

**Fig. 6.** Possible BPA degradation pathways during PS/UV-C and rGO/PS/UV-C treatments. The degradation products **4'-hydroxy-acetophenone** and **benzoquinone** were not observed during rGO/PS/UV-C treatment.

prone to hydrogen addition/abstraction, while SO_4^{2-} preferably react with benzene-containing compounds by an electron transfer mechanism. Table 2 presents the identified and unidentified degradation products obtained during PS/UV-C and rGO/PS/UV-C treatments of BPA-spiked TWW at different treatment time intervals by UPLC-Q-TOF-MS analysis. Five aromatic intermediates together with eight unidentified ones were evidenced for the investigated treatment processes.

BPA degradation via PS/UV-C yielded eleven observed products, while a total of seven products were qualified during rGO/PS/UV-C treatment. The chemical structures of the identified degradation products for PS/UV-C treatment were determined as 2-(4-hydroxyphenyl)-propanol-2-ol, 4-hydroxyacetophenone, 4-isopropylphenol, p-isopropenyl phenol and benzoquinone. The ESI mass spectra of these identified degradation products were provided in Supporting Information Fig. S1.

However, during rGO/PS/UV-C treatment of BPA, 4-hydroxyacetophenone and benzoquinone were not observed. It should be emphasized here that the concentration p-isopropenyl phenol, which was evidenced in both processes, linearly increased throughout the treatment period. As can be seen from Table 2, some intermediates mainly the unidentified ones, had molecular sizes greater than that of BPA. Oxidative coupling reactions and the addition of HO^{\cdot} and $\text{SO}_4^{\cdot-}$ to neutral molecules could result higher molecular weight degradation products are quite common [39]. In the present study however, none of the evidenced unidentified degradation products could be associated with the oxidative degradation products of BPA. The chromatographic peak area of these unidentified degradation products fluctuated through the investigated treatment systems except DP2, which was steadily increased during both PS/UV-C and rGO/PS/UV-C processes. One should keep in mind that the real TWW is a very complex medium and contains a variety of natural organic matter (humic + fulvic acids, etc.) together with refractory pollutants and biologically inert metabolites, etc. that might have ended up with the appearance of several unidentified degradation products. The similarity in the qualified degradation products, although not being fully interpreted, indicates some similarities in degradation pathways of BPA treatment by the PS/UV-C and rGO/PS/UV-C systems. Considering the aforementioned results and taking into consideration of the previously reported degradation pathways of free radical-based oxidation of BPA, it could be concluded that BPA degradation by the PS/UV-C and rGO/PS/UV-C treatment systems proceeded through hydroxylation and oxidation of the aromatic ring and alkyl groups to the corresponding phenolic, quinonic, aldehyde and carboxylic acid structures such as formic, acetic and oxalic acids [7,13]. Based on the present experimental results and the previous related work [7,13,38,40], the proposed degradation pathway of BPA via PS/UV-C and rGO/PS/UV-C treatment systems is given in Fig. 6.

3.5. Quenching studies for rGO/PS/UV-C treatment

Two sets of quenching experiments were carried out with the well-known free radical probe chemicals TBA and EtOH to elucidate the dominant reactive oxygen species of the rGO/PS/UV-C treatment process. The quenching agents were separately added at a concentration of 70.4 mM to obtain a relative probe chemical:BPA molar ratio of 8000:1 in the reaction solution. Fig. 7 depicts normalized BPA values observed during rGO/PS/UV-C treatment in TWW in absence and presence of either TBA or EtOH together with the calculated BPA decay rate coefficients. As is obvious from Fig. 7, BPA abatements are dramatically inhibited in the presence of the probe chemicals; however, the inhibitory effect of EtOH is stronger. After 30 min rGO/PS/UV-C treatment, BPA removals dropped to 59% and 38% upon TBA and EtOH addition, respectively. Inhibition of BPA removal rates were calculated as 87% and 95% in the presence of TBA and EtOH, respectively, on the basis of BPA abatement rate coefficients (shown in Fig. 7 Caption), respectively. Since EtOH inhibition of BPA oxidation was more pronounced than TBA inhibition (Fig. 7), it might be inferred that both radicals play a pivotal role in BPA degradation, however, the presence and role of $\text{SO}_4^{\cdot-}$ might be dominating over HO^{\cdot} . This finding is also consistent with previous related work postulating that $\text{SO}_4^{\cdot-}$ are mainly involved in the treatment systems with PS activation [13,15,17]. It should also be pointed out here that the quenching studies were conducted in real effluent, such that multiple effects of organic and inorganic water constituents should be accounted for when evaluating the effects of free radical scavengers.

3.6. Assessment of toxicity

It has been reported that during application of advanced oxidation processes, degradation intermediates being more inhibitory (toxic) than the original (micro)pollutant might form and accumulate in the

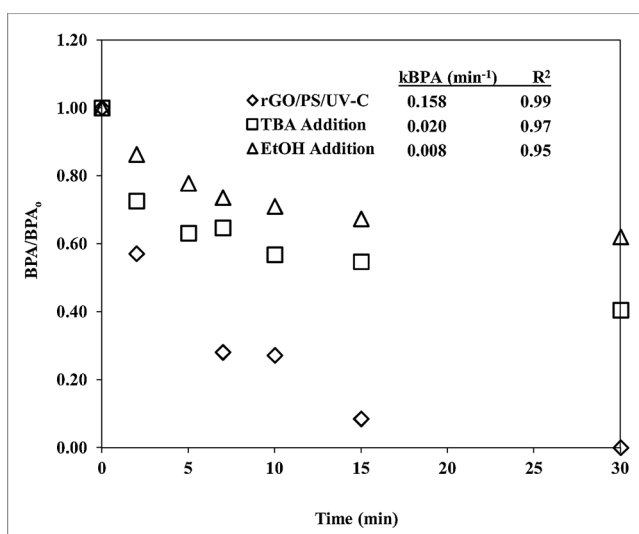


Fig. 7. Effect of TBA and EtOH free radical probe chemicals on BPA abatements (normalized plots) during rGO/PS/UV-C treatment in TWW. Reaction conditions: BPA = 2 mg/L (8.8 μM); DOC (BPA + TWW) = 8.6 mg/L; PS = 0.125 mM; TBA = EtOH = 70.4 mM; rGO = 0.01 g/L; I_0 = 2.6 W/m²; pH = 7.5.

reaction medium [17,39]. Hence, it is crucial to follow changes in toxicity preferably by means of a battery test or at least with a standardized bioassay using representative microorganisms to ensure eco-toxicological safety during application of new/emerging treatment processes. For this purpose, in the present study, acute toxicity (bioluminescence inhibition) tests were undertaken with BPA-spiked TWW being subjected to rGO/PS/UV-C and PS/UV-C treatments. Fig. 8 presents percent relative *V. fischeri* inhibition values (%) measured during 30 min rGO/PS/UV-C and PS/UV-C treatments of BPA-spiked TWW. The original ($t = 0$ min) relative inhibition rate was already low (19%), and dropped promptly to 6% after 5 min rGO/PS/UV-C treatment. As the treatment process progressed, a minor fluctuation (rise to 8% and drop to 3% at the end of treatment) occurred; however, the obtained inhibition values reveal that no toxic degradation intermediates were formed during rGO/PS/UV-C treatment of BPA in TWW. For the PS/UV-

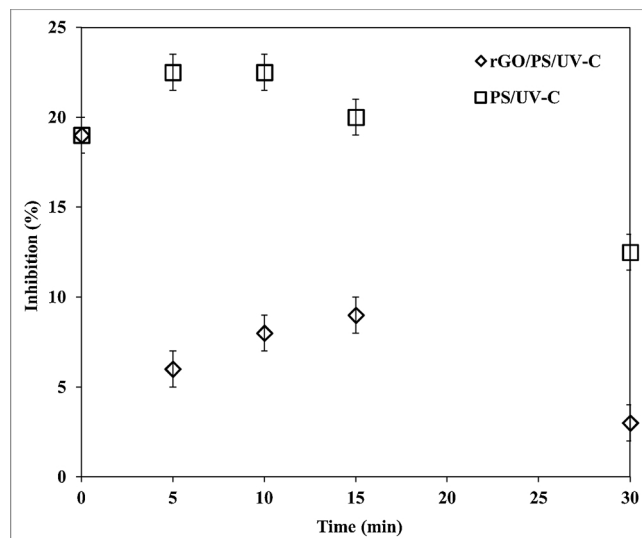


Fig. 8. Percent relative *V. fischeri* inhibition values for rGO/PS/UV-C and PS/UV-C treatments of BPA-spiked TWW. Reaction conditions: BPA = 2 mg/L (8.8 μM); DOC (BPA + TWW) = 8.6 mg/L; PS = 0.125 mM; rGO = 0.01 g/L; I_0 = 2.6 W/m²; pH = 7.5.

C treatment process, on the other hand, percent inhibition rates were appreciably higher; during the course of treatment, inhibition values increased from 19% (at $t = 0$ min) to 22.5% (5th and 10th min), and thereafter decreased slowly to 20% (15th min) and finally to 12.5% at the end of 30 min photochemical treatment. The toxicity results support the findings that some degradation intermediates evolved during rGO/PS/UV-C and PS/UV-C treatments of BPA-spiked TWW were similar but appeared at different reaction times. This is also consistent with the obtained BPA-DOC removal rates for rGO/PS/UV-C and PS/UV-C, where the former process appeared to be kinetically faster. Due to the fact that the rGO/PS/UV-C treatment combination involving oxidation and adsorption resulted in higher removal efficiencies as compared with the PS/UV-C treatment system, it is not surprising that *V. fischeri* inhibition rates were found significantly lower for rGO/PS/UV-C treatment. Again, it should be noted here that the water matrix (TWW) is expected to influence toxicity results, and inorganic-organic TWW (see Table 1) components might have additive, stimulating/synergistic effects on inhibition rates.

4. Conclusions

The effect of home-made reduced graphene oxide (rGO) nanoparticles on the photochemical treatment of bisphenol A (BPA) with the persulfate/UV-C process in real tertiary wastewater was investigated. From the experimental study it could be concluded that rGO acts as an adsorbent and persulfate activator and thus enhances the oxidation reaction of the PS/UV-C treatment process appreciably. All followed environmental parameters such as mother pollutant and dissolved organic carbon removal rates as well as percent bioluminescence inhibition rates were appreciably improved during PS/UV-C treatment in the presence rGO. According to the free radical quenching study, sulfate radicals are dominating over hydroxyl radicals in terms of BPA degradation. Several common degradation products could be identified for PS/UV-C and rGO/PS/UV-C treatments, whereas some slight differences in structure and appearance were also evidenced. Assessment of rGO surface properties delineated that the chemical composition of rGO was modified after photochemical treatment of BPA-spiked effluent.

Acknowledgements

This Special Issue is dedicated to honor the retirement of Prof. César Pulgarin at the Swiss Federal Institute of Technology (EPFL, Switzerland), a key figure in the area of Catalytic Advanced Oxidation Processes. Prof. Pulgarin was and will always be our inspiration in photocatalytic treatment applications. The authors are thankful to Mrs. Elif Öztürk for her technical assistance in the instrumental analyses of bisphenol A degradation products. The technical support of Prof. Sebahattin Gurmen and Res. Assist. Duygu Yesiltepe Ozcelik in rGO surface analyses is also deeply appreciated.

References

- M. Noszczyńska, Z. Piotrowska-Seget, Bisphenols: application, occurrence, safety, and biodegradation mediated by bacterial communities in wastewater treatment plants and rivers, *Chemosphere* 201 (2018) 214–223, <https://doi.org/10.1016/j.chemosphere.2018.02.179>.
- J.M. Pahigian, Y. Zuo, Occurrence, estrogen-related bioeffects and fate of bisphenol a chemical degradation intermediates and impurities: a review, *Chemosphere* 207 (2018) 469–480, <https://doi.org/10.1016/j.chemosphere.2018.05.117>.
- M. Ashfaq, Q. Sun, H. Zhang, Y. Li, Y. Wang, M. Li, M. Lv, X. Liao, C.-P. Yu, Occurrence and fate of bisphenol a transformation products, bisphenol a mono-methyl ether and bisphenol a dimethyl ether, in wastewater treatment plants and surface water, *J. Hazard. Mater.* 357 (2018) 401–407, <https://doi.org/10.1016/j.jhazmat.2018.06.022>.
- L.-H. Wu, X.-M. Zhang, F. Wang, C.-J. Gao, D. Chen, J.R. Palumbo, Y. Guo, E.Y. Zeng, Occurrence of bisphenol S in the environment and implications for human exposure: a short review, *Sci. Total Environ.* 615 (2018) 87–98, <https://doi.org/10.1016/j.scitotenv.2017.09.194>.
- W. Chen, C. Zou, Y. Liu, X. Li, The experimental investigation of bisphenol a degradation by fenton process with different types of cyclodextrins, *J. Ind. Eng. Chem.* 56 (2017) 428–434, <https://doi.org/10.1016/j.jiec.2017.07.042>.
- H. Guo, N. Jiang, J. Li, Y. Wu, Synergistic degradation of bisphenol a by pulsed discharge plasma with granular activated carbon: effect of operating parameters, synergistic mechanism and possible degradation pathway, *Vacuum* 156 (2018) 402–410, <https://doi.org/10.1016/j.vacuum.2018.07.044>.
- T. Olmez-Hancı, I. Arslan-Alaton, B. Genc, Bisphenol a treatment by the hot persulfate process: oxidation products and acute toxicity, *J. Hazard. Mater.* 263 (2013) 283–290, <https://doi.org/10.1016/j.jhazmat.2013.01.032>.
- S. Giannakis, F.A.G. Vives, D. Grandjean, A. Magnet, L.F. De Alencastro, C. Pulgarin, Effect of advanced oxidation processes on the micropollutants and the effluent organic matter contained in municipal wastewater previously treated by three different secondary methods, *Water Res.* 84 (2015) 295–306, <https://doi.org/10.1016/j.watres.2015.07.030>.
- K. Intarasuwan, P. Amornpitoksuk, S. Suwanboon, P. Graidist, S. Maungchanburi, C. Randorn, Effect of Ag loading on activated carbon doped ZnO for bisphenol a degradation under visible light, *Adv. Powder Technol.* 29 (2018) 2608–2615, <https://doi.org/10.1016/j.aptech.2018.07.006>.
- P.V.L. Reddy, K.-H. Kim, B. Kavitha, V. Kumar, N. Raza, S. Kalagara, Photocatalytic degradation of bisphenol a in aqueous media: a review, *J. Environ. Manage.* 213 (2018) 189–205, <https://doi.org/10.1016/j.jenvman.2018.02.059>.
- V. Vaiano, G. Iervolino, L. Rizzo, Cu-doped ZnO as efficient photocatalyst for the oxidation of arsenite to arsenate under visible light, *Appl. Catal. B* 238 (2018) 471–479, <https://doi.org/10.1016/j.apcatb.2018.07.026>.
- Y. Zhang, F. Wang, P. Ou, H. Zhu, Y. Lai, Y. Zhao, W. Shi, Z. Chen, S. Li, T. Wang, High efficiency and rapid degradation of bisphenol a by the synergy between adsorption and oxidization on the MnO₂@nano hollow carbon sphere, *J. Hazard. Mater.* 360 (2018) 223–232, <https://doi.org/10.1016/j.jhazmat.2018.08.003>.
- B. Darsinou, Z. Frontistis, M. Antonopoulou, I. Konstantinou, D. Mantzavinos, Sono-activated persulfate oxidation of bisphenol a: kinetics, pathways and the controversial role of temperature, *Chem. Eng. J.* 280 (2015) 623–633, <https://doi.org/10.1016/j.cej.2015.06.061>.
- F. Gao, Y. Li, B. Xiang, Degradation of bisphenol a through transition metals activating persulfate process, *Ecotoxicol. Environ. Saf.* 158 (2018) 239–247, <https://doi.org/10.1016/j.ecoenv.2018.03.035>.
- Y.-G. Kang, H.C. Vu, T.T. Le, Y.-S. Chang, Activation of persulfate by a novel Fe(II)-immobilized chitosan/alginate composite for bisphenol a degradation, *Chem. Eng. J.* 353 (2018) 736–745, <https://doi.org/10.1016/j.cej.2018.07.175>.
- J. Yan, M. Lei, L. Zhu, M.N. Anjum, J. Zou, H. Tang, Degradation of sulfamonomethoxine with Fe₃O₄ magnetic nanoparticles as heterogeneous activator of persulfate, *J. Hazard. Mater.* 186 (2011) 1398–1404, <https://doi.org/10.1016/j.jhazmat.2010.12.017>.
- T. Olmez-Hancı, I. Arslan-Alaton, Sulfate radical based advanced oxidation processes for the removal of endocrine disrupting compounds, in: D.G. Mita (Ed.), *Endocrine Disruptors and Their Effect on Environment and Human Health*, Research Signpost, Trivandrum, Kerala, 2018, pp. 65–105.
- S. Chowdhury, R. Balasubramanian, Recent advances in the use of graphene-family nanoadsorbents for removal of toxic pollutants from wastewater, *Adv. Colloid Interface Sci.* 204 (2014) 35–56, <https://doi.org/10.1016/j.cis.2013.12.005>.
- T. Jiang, J. Li, Z. Sun, X. Liu, T. Lu, L. Pan, Reduced graphene oxide as co-catalyst for enhanced visible light photocatalytic activity of BiOBr, *Ceram. Int.* 42 (2016) 16463–16468, <https://doi.org/10.1016/j.ceramint.2016.06.079>.
- Y. Guo, Z. Zeng, Y. Zhu, Z. Huang, Y. Cui, J. Yang, Catalytic oxidation of aqueous organic contaminants by persulfate activated with sulfur-doped hierarchically porous carbon derived from thiophene, *Appl. Catal. B* 220 (2018) 635–644, <https://doi.org/10.1016/j.apcatb.2017.08.073>.
- J. Kang, X. Duan, L. Zhou, H. Sun, M.O. Tadé, S. Wang, Carbocatalytic activation of persulfate for removal of antibiotics in water solutions, *Chem. Eng. J.* 288 (2016) 399–405, <https://doi.org/10.1016/j.cej.2015.12.040>.
- X. Duan, Z. Ao, H. Sun, S. Indrawirawan, Y. Wang, J. Kang, F. Liang, Z.H. Zhu, S. Wang, Nitrogen-doped graphene for generation and evolution of reactive radicals by metal-free catalysis, *ACS Appl. Mater. Interfaces* 7 (2015) 4169–4178, <https://doi.org/10.1021/am508416n>.
- A.L. Higginbotham, D.V. Kosynkin, A. Sinitskii, Z. Sun, J.M. Tour, Lower-defect graphene oxide nanoribbons from multiwalled carbon nanotubes, *ACS Nano* 4 (2010) 2059–2069, <https://doi.org/10.1021/nn100118m>.
- L. Lin, H. Wang, P. Xu, Immobilized TiO₂-reduced graphene oxide nanocomposites on optical fibers as high performance photocatalysts for degradation of pharmaceuticals, *Chem. Eng. J.* 310 (2017) 389–398, <https://doi.org/10.1016/j.cej.2016.04.024>.
- D.C. Marcano, D.V. Kosynkin, J.M. Berlin, A. Sinitskii, Z. Sun, A. Slesarev, L.B. Alemany, W. Lu, J.M. Tour, Improved synthesis of graphene oxide, *ACS Nano* 4 (2010) 4806–4814, <https://doi.org/10.1021/nn1006368>.
- L.V. Nguyen, R. Busquets, S. Ray, A.B. Cundy, Graphene oxide-based degradation of metaldehyde: effective oxidation through a modified Fenton's process, *Chem. Eng. J.* 307 (2017) 159–167, <https://doi.org/10.1016/j.cej.2016.08.052>.
- W.-C. Hou, S. BeigzadehMilani, C.T. Jafvert, R.G. Zepp, Photoreactivity of unfunctionalized single-wall carbon nanotubes involving hydroxyl radical: chiral dependency and surface coating effect, *Environ. Sci. Technol.* 48 (2014) 3875–3882, <https://doi.org/10.1021/es500013j>.
- Z.-H. Diao, Wei-Qian, P.-R. Guo, L.-J. Kong, S.-Y. Pu, Photo-assisted degradation of bisphenol a by a novel FeS₂@SiO₂ microspheres activated persulfate process: synergistic effect, pathway and mechanism, *Chem. Eng. J.* 349 (2018) 683–693, <https://doi.org/10.1016/j.cej.2018.05.132>.
- J.G. Radich, A.L. Krenselewski, J. Zhu, P.V. Kamat, Is graphene a stable platform for

photocatalysis? Mineralization of reduced graphene oxide with UV-irradiated TiO_2 nanoparticles, *Chem. Mater.* 26 (2014) 4662–4668, <https://doi.org/10.1021/cm5026552>.

[30] X. Duan, C. Su, L. Zhou, H. Sun, A. Suvorova, T. Odedairo, Z. Zhu, Z. Shao, S. Wang, Surface controlled generation of reactive radicals from persulfate by carbocatalysis on nanodiamonds, *Appl. Catal., B* 194 (2016) 7–15, <https://doi.org/10.1016/j.apcatb.2016.04.043>.

[31] T. Olmez-Hancı, I. Arslan-Alaton, S. Gurmen, I. Gafarlı, S. Khoei, S. Safaltn, D. Yesiltepe Ozcelik, Oxidative degradation of bisphenol a by carbocatalytic activation of persulfate and peroxymonosulfate with reduced graphene oxide, *J. Hazard. Mater.* 360 (2018) 141–149, <https://doi.org/10.1016/j.jhazmat.2018.07.098>.

[32] I. Arslan-Alaton, O. Kolba, T. Olmez-Hancı, Removal of an X-ray contrast chemical from tertiary treated wastewater: investigation of persulfate-mediated photochemical treatment systems, *Catal. Today* 313 (2018) 134–141, <https://doi.org/10.1016/j.cattod.2017.11.002>.

[33] World Health Organization (WHO), *Sulfate in Drinking-Water, Background Document for Development of WHO Guidelines for Drinking-Water Quality*, WHO/SDE/WSH/03.04./114, Geneva, 2004.

[34] N.E. Sorokina, M.A. Khaskov, V.V. Avdeev, I.V. Nikol'skaya, Reaction of graphite with sulfuric acid in the presence of KMnO_4 , *Russ. J. Gen. Chem.* 75 (2005) 162–168.

[35] ISO 11348-3, Water Quality - Determination of the Inhibitory Effect of Water Samples of the Light Emission of *Vibrio fischeri* (Luminescent Bacteria Test) Part 3: Method Using Freeze-Dried Bacteria, International Organization for Standardization (ISO), Geneva, 2007 2007.

[36] T. Olmez-Hancı, I. Arslan-Alaton, D. Dursun, Investigation of the toxicity of common oxidants used in advanced oxidation processes and their quenching agents, *J. Hazard. Mater.* 278 (2014) 330–335, <https://doi.org/10.1016/j.jhazmat.2014.06.021>.

[37] APHA/AWWA/WPCF, *Standard Methods for the Examination of Water and Wastewater*, 22nd ed., American Public Health Association (APHA), Washington, DC, 2012.

[38] C. Liang, H.-W. Su, Identification of sulfate and hydroxyl radicals in thermally activated persulfate, *Ind. Eng. Chem. Res.* 48 (2009) 5558–5562, <https://doi.org/10.1021/ie9002848>.

[39] T.X.H. Le, T. Van Nguyen, Z.A. Yacouba, L. Zoungrana, F. Avril, D.L. Nguyen, E. Petit, J. Mendret, V. Bonniol, M. Bechelany, S. Lacour, G. Lesage, M. Cretin, Correlation between degradation pathway and toxicity of acetaminophen and its by-products by using the electro-fenton process in aqueous media, *Chemosphere* 172 (2017) 1–9, <https://doi.org/10.1016/j.chemosphere.2016.12.060>.

[40] J. Poerschmann, U. Trommler, T. Górecki, Aromatic intermediate formation during oxidative degradation of bisphenol a by homogeneous sub-stoichiometric fenton reaction, *Chemosphere* 79 (2010) 975–986, <https://doi.org/10.1016/j.chemosphere.2010.03.030>.